

1 *Numerical Analysis of Longwall Mining Layout*  
2 *for a Wyoming Trona Mine*

3 A.G. Corkum<sup>a,\*</sup> and M.P. Board<sup>b</sup>

4 <sup>a</sup>*Department of Civil and Resource Engineering, Dalhousie University,*  
5 *1360 Barrington St., Rm D215, PO Box 15000, Halifax, NS, Canada, B3H 4R2*

6  
7 <sup>b</sup>*Hecla Limited, 6500 N. Mineral Drive, Suite 200,*  
8 *Coeur d'Alene, ID, United States, 83815-9408*

9 *\*Corresponding Author: Tel. +1 902 494-3960; Email Address: andrew.corkum@dal.ca*

---

10 **Abstract**

11 At Solvay Mine, located in southwestern Wyoming, a subhorizontal trona  
12 seam is mined at depths of between 460-490 m using mechanized room-and-pillar  
13 and longwall mining methods. The stratigraphy at the mine generally consists of  
14 horizontally laminated (*i.e.*, bedded) sedimentary rocks comprised mostly of  
15 shales and sandstones with significantly contrasting mechanical properties. Most  
16 notably, a 43 – 82 m-thick massive, brittle sandstone unit (Tower Sandstone) is  
17 located approximately 100 m above the mining level. The Tower Sandstone unit  
18 has a tendency to promote stress arching within the overburden rock that can  
19 bridge over panel-scale mine instabilities and can lead to violent multi-panel  
20 collapse failure. One such violent collapse is the well-documented 5.1 magnitude  
21 seismic event due to a 1 x 2 km multi-panel failure on February 3, 1995. It has  
22 proven difficult to account for this arching behaviour with conventional mine  
23 design methods, such as the tributary area method. Therefore, over the past two  
24 decades or more, Solvay Mine has been utilizing numerical modelling techniques  
25 along with field instrumentation/monitoring as part of an integrated program to  
26 gain an enhanced understanding of the complex response of the overlying

27 stratigraphy (*i.e.*, arching) to mining. In 2005 and 2006, several longwall panels in  
28 the northwest and southeast areas of the mine were instrumented and monitored  
29 during mining. Two- and three-dimensional numerical models, using *FLAC* and  
30 *FLAC3D*, were developed and calibrated on the basis of the instrumentation data,  
31 and these models were then used for mine design verification (*e.g.*, pillar and  
32 panel dimensions). This mining case study illustrates the complex excavation  
33 response due to the contrasts in stratigraphy at Solvay Mine and presents a  
34 numerical modelling study that captures the dominant aspects of these conditions.  
35 In addition, the practical use and role of numerical modelling and instrumentation  
36 within an integrated mine design methodology is demonstrated.

37

38       **Keywords:** longwall mining, trona, subsidence, instrumentation,  
39 numerical modelling, *FLAC*

40

41 **1. Introduction**

42 Trona is a non-marine evaporite mineral composed of sodium  
43 sesquicarbonate that has a major use in the production of glass, chemicals, paper  
44 and detergents. Trona has been mined continuously in several mines in the Green  
45 River Basin since 1947 using numerous mining methods. One of the main sources  
46 of trona production in the Green River Basin is Solvay Mine, located in western  
47 Wyoming, approximately 6.5 km east of Little America and south of Interstate 80.

48 At Solvay Mine, a 2.7 m-thick, sub-horizontal trona seam, known as  
49 Bed 17, is mined at depths of approximately 460 – 490 m. The general  
50 stratigraphy consists of horizontally laminated (*i.e.*, bedded) sedimentary rocks  
51 with significant contrasts in stiffness and brittleness, most notably the massive 43  
52 – 82 m thick Tower Sandstone unit located within the bottom third of the  
53 overburden profile. The contrast in mechanical characteristics of the geological  
54 units result in complex behaviour of the mine openings and overlying strata, such  
55 as stress arching and progressive failure with mining advance. This behaviour  
56 significantly impacts the evolution of the stress distribution, yielding and  
57 subsidence within the strata. Conventional mine design methods, such as tributary  
58 area theory and empirical pillar design curves, do not account for such behaviour.  
59 The most critical issue is violent failure of the massive, brittle Tower Sandstone  
60 as a result of “stress arching” across multiple mine panels leading to a delayed  
61 failure. One example of this type of failure is the well-documented 5.1 magnitude  
62 seismic event due to a large (1 x 2 km), violent, multi-panel failure on February 3,  
63 1995 [1-4].

64 For the past two decades, numerical modelling methods have been utilized  
65 at Solvay Mine to evaluate the excavation-scale and mine-scale mining response  
66 and performance. Over this period, an increasing level of experience and insight  
67 into the relatively complex rock mechanics behaviour has been gained from  
68 observations of mine response, and instrumentation and monitoring. However,  
69 given the complexity of overburden’s response to mining and the consequence of

70 inaccurate predictions in mine design, it is critical to ensure the design model is  
71 calibrated.

72 In 2005 and 2006, Solvay Mine completed mining four longwall panels in  
73 the northwest portion (“NW District”) of the mine and began mining a longwall  
74 panel in the southeast area (“SE District”) of the mine. An overall plan of Solvay  
75 Mine showing the location of these Districts is provided in Fig. 1. These longwall  
76 panels were monitored for surface subsidence (geodetic monitoring), pillar  
77 stresses (IRAD stressmeters), and downhole extensional strain (time domain  
78 reflectometry: TDR cable). The monitoring data was used to carry out detailed  
79 back analysis of the longwall mining to develop a “calibrated” numerical model  
80 using the two-dimensional continuum code *FLAC* [5]. The model was further  
81 verified using a three-dimensional *FLAC3D* [6] model of early stage mining of  
82 the SE District longwall panels.

83 This mining case study demonstrates the practical use and role of  
84 numerical modelling and instrumentation within an integrated mine design  
85 methodology. In addition, it illustrates the complex excavation response from  
86 longwall mining the relatively deep, horizontal trona seam beneath a stratigraphic  
87 profile containing units with significantly contrasting mechanical properties.

88 It should be noted that the original monitoring data and numerical  
89 modelling presented in this study were carried out using imperial units [7]. The  
90 imperial units have been converted to metric for this publication and many of the  
91 originally rounded imperial-based values reported may appear as “odd” values as  
92 a result of unit conversion.

## 93 **2. Background**

94 Over the last two decades numerous numerical modelling-based studies  
95 have been carried out at Solvay Mine and other mining operations in the  
96 immediate vicinity of Solvay Mine [3,8-11]. This section provides a brief  
97 overview of the general conditions at Solvay Mine, such as the geological

98 conditions, rock mechanics conditions, and summarizes the key mining-related  
99 observations from these past studies.

## 100 **2.1 Geological Setting**

101 The Green River Formation has a maximum thickness of approximately  
102 730 m in the Green River Basin and consists primarily of horizontally bedded  
103 fine-grained mudstones, siltstone, marlstone and oilshale [12]. The Green River  
104 Formation is comprised of the lower Tipton Shale Member, the middle Wilkins  
105 Peak Member and the upper Laney Shale Member. The bedded trona units occur  
106 within the Wilkins Peak Member. The units were deposited during the Eocene in  
107 a large lake in the Green River Basin. The evaporite units (*e.g.*, halite and trona)  
108 were formed during evaporative periods and the oilshale units were formed during  
109 high water stages when organic organisms (*i.e.*, algae) flourished. A total of  
110 twenty-two significant trona beds, including Bed 17, are present within the  
111 Wilkins Peak Member.

112 The Tower Sandstone is a massive, or irregularly bedded, sandstone unit  
113 that derives its name from capping the erosional remnants called “The Towers”  
114 [13] located north of Green River. The Tower Sandstone is part of the lower  
115 Laney Shale Member at the Wilkins Peak-Laney Shale contact. The Tower  
116 Sandstone is comprised of approximately 75% detrital material, of which 40% is  
117 quartz and 25% is cementitious material [14]. According to Culbertson [15], the  
118 Tower Sandstone was laid down as a marginal deposit of the fluctuating fresh  
119 water lake in the Green River Basin.

120 The stratigraphy at Solvay Mine, where the approximately 3.3 m thick  
121 Bed 17 trona seam is mined, is comprised of the aforementioned units. The Bed  
122 17 trona seam is underlain by a weak oilshale layer (approximately 2 m thick) and  
123 overlain by a bedded shale unit. Approximately 20 m above Bed 17 is a 10 m-  
124 thick sandstone/mudstone layer known as the D Sandstone. The Tower Sandstone  
125 unit, a generally strong and brittle layer ranging between 40 and 82 m thick across  
126 the mine site, is encountered about 90 to 122 m above Bed 17. The Upper Wilkins

127 Peak member is found between the D and Tower Sandstone units and consists of  
128 bedded shale and mudstone sequences.

129 The Tower Sandstone is about 82 m thick in the vicinity of the NW  
130 District, while in the SE District, based on mapped stratigraphy of Shaft 6 located  
131 near the SE District, it is approximately half that thickness (41 m thick) [16]. The  
132 thickness of the Tower in the SE District depends on whether the lower portion of  
133 the unit, up to about 18 to 24 m thick and described as more fractured and with  
134 shale interbedding, is included in the interpreted thickness of the Tower  
135 Sandstone unit. Furthermore, the depth from ground surface to Bed 17 is greater  
136 in the SE District than in the NW District. A comparison of the stratigraphy at  
137 both SE and NW Districts are shown in Fig. 2.

## 138 **2.2 Mine Layout**

139 As show in Fig. 1, longwall panels in the NW District were oriented in a  
140 north-south direction. These panels were 165 m wide and 1525 m long with 39 m-  
141 wide gateroad pillars and, with the exception of the western-most panel, which  
142 was 152 m wide. In general, performance of pillars and openings in the NW  
143 District due to longwall mining was considered to be good with few signs of  
144 stress-related instability in the gateroads or the face. The longwall panels in the  
145 NW District were mined from east to west.

## 146 **2.3 Past Observations of Rock Mechanics Mining Response**

147 Although the horizontally bedded geological structure at Solvay Mine is  
148 not overly complex, the high contrasts in strength and stiffness of some of the  
149 units does result in a complex response to mining. There are several important  
150 factors that control the mining response at Solvay and other mines in the Green  
151 River area. These include: a) panel extraction ratio; b) panel span; c) barrier pillar  
152 thickness; d) strength of the floor-pillar system; and e) the thickness, strength and  
153 brittleness of the Tower Sandstone. Based on field observations, instrumentation  
154 and the results of past numerical analysis, Board and Damjanac [11] describe the

155 mechanism of caving and subsidence for longwall mining at Solvay Mine as  
156 follows.

157           Near-vertical shear fracture propagation occurs above the abutments in the  
158 weak shales (immediate roof and Upper Wilkins Peak Member), resulting in  
159 uniform downward movement of the shale beds with little internal vertical  
160 straining until they contact the floor. The subsequent shale collapse opens a  
161 significant gap beneath the Tower Sandstone (up to a meter or more wide) with a  
162 span nearly the width of the panel. Bending of the Tower Sandstone into this gap  
163 occurs, with resulting formation of a zone of tension within the base of the Tower  
164 Sandstone where it has become unconfined. This tensile zone results in bulking  
165 and progressive collapse of the Tower Sandstone base. The failure of the Tower  
166 Sandstone is typically non-violent in this case, because it is essentially unconfined  
167 at its base and subject to progressive failure under low or tensile stresses. This  
168 would probably result in progressive block failures from the base of the unit that  
169 would advance, or “run,” vertically upwards until the accumulation of bulked  
170 collapse material arrested further advancement of failure. Subsequent units  
171 overlying the Tower Sandstone then translate vertically downward in response to  
172 bending of the Tower Sandstone. This translation occurs with little internal strain  
173 and damage to the downward moving block. However, bedding planes within the  
174 Bridger Formation often undergo bedding plane shearing of several centimeters as  
175 the units subside. Mining of multiple panels results in the Tower Sandstone  
176 bending over all panels, creating a single subsidence trough with no evidence of  
177 the impact of chain pillars. A “break line” defining the angle of draw of the  
178 subsidence trough forms through all units at an angle of approximately 70° from  
179 the horizontal.

180           Within Bed 17, the contrast between the relatively strong and brittle trona,  
181 and the weak and ductile oilshale floor results in a unique load response  
182 behaviour of mine pillars and openings that has been well documented by Board  
183 et al. [3]. As the pillar punches into weak floor oilshale, the oilshale are squeezed

184 out beneath the pillar in a ductile manner, and the pillar is then pulled apart at its  
185 base. Rib rash fractures develop at the floor line and the beds buckle in the room  
186 centers. Continued punching drives a wedge-shaped central pillar core into the  
187 floor. This core is highly confined and can result in pillar strengthening.  
188 Therefore, the pillar-floor must be treated as a “system response” to loading. This  
189 pillar load response is of greater significance for relatively slender pillars in room-  
190 and-pillar mining than for longwall mining.

191 One of the objectives of longwall mining at Solvay Mine is to induce a  
192 “controlled failure” of the Tower Sandstone and avoid conditions with potential  
193 for delayed, violent failure. In general, this appears to have been achieved in the  
194 NW District. Moreover, given the thickness of the overlying Tower Sandstone  
195 (82 m), the strength of the oilshale floor and roof shales, and the mining  
196 dimensions used, longwall mining in the NW District has performed adequately.  
197 The gob seems to have developed gradually without undue signs of violent  
198 collapse. Gateroads and chain pillars have shown few signs of stress-induced  
199 distress.

### 200 **3. Geotechnical Conditions**

201 There have been several rock mechanics laboratory programs carried out  
202 on the geological units in the Green River area to evaluate the intact (*i.e.*,  
203 laboratory scale) rock properties by the various mines and their consultants. The  
204 most detailed laboratory study was conducted by Tetra Tech Inc. (Salt Lake City)  
205 on behalf of the Joint Industry OGT project [17]. The data from the numerous  
206 rock mechanics studies were compiled by Weller [18] who provided  
207 recommended intact rock Unconfined Compressive Strength (*UCS*) values for the  
208 dominant geological units at Solvay Mine. The intact rock parameters are shown  
209 in Table 1.

210 In order to account for the presence of jointing, fractures and scale effects  
211 (*i.e.*, from laboratory size to field problem size), rock mass properties are used for



212 analysis. Methods to determine Hoek-Brown rock mass properties have been  
 213 developed [19]; however, these relationships are more appropriate for a relatively  
 214 homogeneous, jointed rock mass, rather than the strongly bedded and highly  
 215 variable rock layering that is found in the stratigraphy at Solvay Mine [20]. Based  
 216 on the laboratory test data, estimated values of Geological Strength Index (*GSI*  
 217 [21]) and past experience with numerous analysis and design projects in the Green  
 218 River area, Board et al. [3] provided a range of rock mass properties for the major  
 219 geological units listed in Table 2. In particular, direct observation and back-  
 220 analysis of the oilshale floor-trona pillar system have been extensively used to  
 221 evaluate rock properties.

222 **Table 1 Intact rock properties from Weller [18]**

Unit	Unconfined Compressive Strength (MPa)
Bridger Formation	51
Laney Shale	57
Tower Sandstone	115
Upper Wilkins Peak	16
D Sandstone	66
Roof Shale	42
Bed 17 (Trona)	45
Oilshale	33

223 **Table 2 Estimated *in situ* rock mass properties for sandstones and shales (from [3])**

Unit	<i>GSI</i>	Young's Modulus (GPa)	Cohesion (MPa)	Friction Angle (°)
Upper Wilkins Peak	40-55	5.2-6.9	0.4-0.7	25-28
Laney Shale	40-55	5.2-6.9	1.2-2.3	25-28

Roof Shale	40-55	5.2-6.9	1.8-2.3	25-28
Tower Sandstone	60-70	22.8	5.2-8.6	40-44
Bed 17 (Trona)	60-70	30	9.3	49
Oilshale	40-55	1.2	1.75	20

224 The rock mass parameters listed in Table 2 provide a starting point for  
225 carrying out numerical analysis for Solvay Mine. However, the 2003 – 2006 NW  
226 District longwall mining provides an opportunity to obtain a more complete  
227 understanding of the likely range of behaviour of all of the critical rock units  
228 within the stratigraphic profile. The instrumentation and monitoring program  
229 provided reliable information at both the mining level (stressmeters), at the  
230 ground surface (subsidence), and also within the stratigraphy (TDR's). A back  
231 analysis of the longwall mining that can capture all of the instrumentation data,  
232 plus match key mining observations, would be considered a calibrated model. A  
233 calibrated model is a prerequisite for model-based design [22].

234 The Green River Basin is a region of relatively low horizontal stresses.  
235 The *in situ* stresses have been determined based on past stress measurements  
236 (Solvay personnel, pers. comm.) at Solvay Mine and observations of mine  
237 excavation response. Based on this, a vertical stress gradient of 0.025 MPa/m with  
238 a ratio of horizontal-to-vertical stress in the range of  $K = 0.3$  to  $0.75$  is likely. A  
239 value of  $K = 0.5$  was used for the analyses.

#### 240 **4. Instrumentation Data from NW District Longwall Mining**

241 Four longwall panels were mined in the NW District between 2003 and  
242 2005. Starting from the eastern most panel (1W1N), the longwall panels were  
243 mined in a north-to-south direction, and the four panels (1W1N through 1W4N)  
244 were mined sequentially from east to west. The layout of the panels in the NW  
245 District are shown in Fig. 1 and Fig. 3. As mentioned previously, the gateroads  
246 and mining face performance was generally suitable with these mining  
247 dimensions.

248 **4.1 *Subsurface Subsidence Measurements***

249 Subsidence data, obtained from topographic surveys, was collected from  
250 two stages of longwall mining in the NW District. The subsidence contours are  
251 shown in Fig. 3 for 2005 (2.5 panels excavated) and Spring 2006 (3 panels  
252 excavated). The longwall mining progress corresponding to these two points in  
253 time is also shown in Fig. 3. Subsidence profiles along an east-west oriented  
254 section are shown in Fig. 4.

255 The surface subsidence trough was elongated in a north-south direction  
256 and symmetrical with the maximum subsidence located approximately in the  
257 center of the mined-out area at each measured interval. A maximum subsidence of  
258 between 60 and 76 cm was recorded in 2005 and between 75 and 91 m was  
259 measured in 2006. In general, the subsidence profiles were relatively smooth and  
260 continuous with no surface expression of the chain pillars between panels.

261 Based on the author's experience from several projects in the Green River  
262 area, subsidence does not typically exceed 20 – 30 cm without significant yielding  
263 of the Tower Sandstone. Moreover, limited yielding of the Tower Sandstone  
264 would result in arching of stresses across longwall panels with a resulting smooth  
265 and shallow subsidence trough. Therefore, the steepness of the measured surface  
266 subsidence trough and magnitude of maximum subsidence are both consistent  
267 with significant yielding of the Tower Sandstone. The subsidence trough was  
268 fairly steep in both 2005 and 2006, which indicated that at least partial yielding of  
269 the Tower Sandstone unit had occurred at these mining stages.

270 **4.2 *Pillar Stress Measurements***

271 A total of thirteen IRAD stressmeters were installed in the chain pillars  
272 along cross-cuts prior to mining the longwalls. These instruments provided a  
273 measure of the vertical stress change beginning at the time that each device was  
274 installed. The thirteen instruments were grouped by areas into Area A through D,  
275 each of which comprised between two and four stressmeters. The stressmeters and  
276 area groupings are shown in Fig. 5.

277           The stressmeter data for the thirteen locations is shown in Fig. 6 for the  
278 time period of March 2003 to July 2006. The stressmeters at Area A, in the east  
279 abutment, shows the least mining-induced increase in stress with all measured  
280 stress changes below 3.5 MPa. The stressmeters in Area B, within the chain pillar  
281 between Panel 1W1N and 1W2N, showed mining-induced stress changes up to  
282 about 24 MPa. Area C and D are within the north and middle area of the chain  
283 pillar between 1W2N and 1W3N, respectively. Stress changes greater than  
284 45 MPa were measured at Area C. Data was only available until November 2005  
285 for Area D, when panel 1W3N was partially mined, when stress reached about  
286 17 MPa. It appears that the stress levels in Area D had not stabilized at that time  
287 and would likely continue to rise due to mining of Panel 1W3N. Both Areas C  
288 and D are located within the same chain pillar in the panel center and the shape of  
289 the data curves at Area D is similar (but slightly lower at a given time) to that of  
290 Area C. Therefore, a similar magnitude of stress change could be expected at  
291 Areas C and D.

## 292 **5. Back Analysis of NW District Longwall Mining**

293           The *FLAC* model was calibrated based on a back analysis of the mining of  
294 four longwall panels in the NW District. This section describes development of  
295 the numerical model, calibration of the model parameters and verification of the  
296 Calibrated Model by comparison with actual instrumentation data.

297           An important aspect of longwall mining is the behaviour of the gob, or  
298 failed rock, behind the advancing longwall face. Little is known about the extent  
299 of caved rock above the mining horizon or the properties of the fully and partially  
300 caved material [20]; however, several authors have used different methods to  
301 simulate the behaviour of this fractured and dilated material. Pappas and Mark  
302 [23] estimated gob particle size distribution using photogrammetric methods and  
303 then scaled the grain size curve down in order to perform laboratory tests on an  
304 analogous gob material. O'Connor and Dowding [24] used an early version of

305 *UDEC* software to simulate the effect of discrete fractures on caving behaviour, in  
306 particular, the interface stiffness of the gob material. Deb [25] used the Pappas  
307 and Mark approach for gob stiffness with a two-dimensional finite element model.  
308 In Deb's work gob development was simulated by replacing a given zone, upon  
309 yielding, with a zone having properties consistent with gob material (*i.e.*, stiffness  
310 and stress). Alejano [26] developed a calibrated *FLAC* model to capture longwall  
311 mining of an inclined coal seam in the English coalfields. Pierce et al. [27] have  
312 developed the Synthetic Rock Mass (SRM) method for modelling cave mining  
313 which also could be used for a sophisticated simulation of longwall gob  
314 development in three-dimensions.

315         According to Peng [28], the gob is usually subdivided into two zones: a  
316 lower, Fully Caved Zone and an Upper Fractured Zone. The Fully Caved Zone  
317 can be expected to extend vertically about 2 to 3 times the mining height and  
318 behaves as a granular material with a relatively high void ratio (*i.e.*, bulked  
319 material). For the Solvay Mine panels, this corresponds to a Fully Caved Zone of  
320 about 8 m above the mining seam (just below the D Sandstone) with the Upper  
321 Fractured Zone above that. Even if the Fully Caved Zone was significantly higher  
322 than this, it is relatively small compared to the full stratigraphical section at  
323 Solvay Mine. Moreover, because of the presence of the D Sandstone layer and the  
324 upper Tower Sandstone, both of which have significant potential to arch or bridge  
325 across panels, the overlying strata is dominated by arching and the subsequent  
326 yielding behaviour of the massive Tower Sandstone. Therefore, direct simulation  
327 of the gob material is likely a less critical issue at Solvay Mine than in other  
328 longwall coal mining cases discussed in the literature.

329         The modelling approach used in this work follows the philosophy laid out  
330 by Starfield and Cundall [29] and Hoek et al. [22], where certain simplifications  
331 were used in order to focus on an understanding of the dominant mechanism of  
332 behaviour. Rock mechanics modelling in this case, and in general, is considered a  
333 "data limited problem." It is not therefore prudent to include model details and

334 refinement that exceed the level of understanding of the rock mechanics  
335 conditions. Therefore, overly sophisticated methods of gob simulation we not  
336 using in this stage of analysis.

### 337 ***5.1 Development of a Two-Dimensional Numerical Model***

338 The two-dimensional code *FLAC* is suitable for the back analysis because  
339 the panels are quite long relative to their width and the effect of excavation  
340 advance on subsidence was considered to be minor. As mentioned above,  
341 development of the gob was not directly accounted for in the model. Moreover,  
342 use of the two-dimensional code allowed for more rapid execution of numerous  
343 models and a more comprehensive parametric study could be conducted than  
344 would be possible using a more computationally intensive three-dimensional  
345 code. Three-dimensional modelling will be described later in Section 5.2.

#### 346 ***5.1.1 Geotechnical Model***

347 The horizontally bedded sedimentary units at Solvay Mine are reasonably  
348 well understood from a geological perspective. However, numerous interbedded  
349 rock types are present and many of these have significantly contrasting rock  
350 mechanics characteristics (*e.g.*, the relatively strong, brittle Bed 17 trona and the  
351 weak, ductile oilshale mine floor). It would be unnecessarily difficult to capture  
352 all of the individual rock layers/units in a mine-scale numerical model. Therefore,  
353 a simplified Geotechnical Model was developed where units with similar rock  
354 mechanics behaviour (*e.g.*, strength and stiffness) were grouped together into  
355 Geotechnical Domains. The Geotechnical Domains were assigned overall  
356 representative properties of the individual subunits comprised within each and  
357 these units were then used to develop a numerical model that includes the  
358 important rock mechanics features without excessive complexity and  
359 computational burden.

360 The stratigraphy of the NW District described in Section 2.1 was used to  
361 develop the *FLAC* model where the Tower Sandstone unit was approximately

362 82 m thick. At this location Bed 17 was at a depth of approximately 470 m. The  
363 stratigraphic profile and rock mechanics characteristics of the various units are  
364 known to vary with lateral extent and there are some differences in the  
365 Geotechnical Model between the NW and SE District. The most notable  
366 differences are the thickness of the Tower Sandstone and the depth below surface  
367 of Bed 17 due to topography and the slight overall dip of Bed 17. The  
368 Geotechnical Model at both the NW and SE Districts is based on the simplified  
369 stratigraphy shown in Fig. 2.

### 370 5.1.2 Model Geometry, Boundary and Initial Conditions

371 In order to capture both the observations within Bed 17 and the surface  
372 subsidence for all four longwall panels in a single model, it was necessary to  
373 develop a large mine-scale model of sufficient size to include all NW District  
374 panels. In addition, a significant distance to the lateral boundaries and the bottom  
375 boundary was also required to minimize model boundary effects. The *FLAC*  
376 model for the NW District longwall panels extended approximately 3000 m  
377 horizontally and approximately 746 m vertically. Model zone sizes ranged from  
378 1.4 to 11 m grading from small to large vertically upwards away from Bed 17.  
379 Suitably fine zone resolution in the critical Tower Sandstone unit was required to  
380 allow for accurate prediction of bending and progressive yielding. Discontinuous  
381 model interfaces, capable of yielding and separating, were built into the model at  
382 the contact of each Geotechnical Domain using *FLAC* interface logic. It was  
383 important to allow for true separation of the underlying shale from the Tower  
384 Sandstone in the model (see Section 2.3). The zones making up the four longwall  
385 panels (1W1N through 1W4N) within Bed 17, were identified within the model  
386 geometry. The individual chain pillars were not directly analyzed in the model.  
387 Instead, a solid pillar separating the longwall panels without the gateroad was  
388 used to represent the pillars. The width of the representative pillar will be termed  
389 the *gross pillar width* to quantify pillar widths. For example, an individual chain

390 pillar width of 39 m with 4.6 m wide gateroads results in a gross pillar width of  
391 82.5 m (*i.e.*,  $(39 \times 2) + 4.5 = 82.5$ ). The *FLAC* model layout is shown in Fig. 7.

392 The model base had fixed boundary conditions laterally and vertically  
393 (pinned boundary). The lateral boundaries were fixed laterally and free vertically  
394 (roller boundary). The vertical stresses in the model were input to correspond to a  
395 stress gradient of 0.025 MPa/m with a ratio of horizontal to vertical stresses (*K*) of  
396 0.5 in both the model's in-plane and out-of-plane directions. Groundwater has not  
397 been a significant issue for the mines in the Green River area and no groundwater  
398 pressure was used in the model.

### 399 5.1.3 Constitutive Model

400 The constitutive models describe how the geomaterials will respond to  
401 loading, including yielding and post-peak behaviour. A detailed description of the  
402 constitutive models available in *FLAC* is described in the software manual [5].  
403 Three main constitutive models were utilized in the *FLAC* models: Mohr-  
404 Coulomb; Strain Softening; and Ubiquitous Joint Mohr-Coulomb. The Mohr-  
405 Coulomb (*Mohr*) utilizes a Mohr-Coulomb shear failure envelope with a tensile  
406 strength cut off and perfectly plastic post-peak parameters. The Strain Softening  
407 (*SS*) model is similar to the *Mohr* model, but also includes strain softening post-  
408 peak parameters. The Ubiquitous Joint Mohr-Coulomb (*SUBI*): is similar to the  
409 *SS* model, but includes preferentially weak planes in a specified orientation that  
410 responds as if there was a continual array (*i.e.*, ubiquitous) of horizontal bedding  
411 planes. The strength of the weak planes is defined by a Mohr-Coulomb failure  
412 criterion. For the *SS* and *SUBI* models, both peak and post-peak residual strength  
413 parameters were specified. The rate at which the strength of the rock mass  
414 decreases after the peak strength is exceeded is a function of the plastic shear  
415 strain ( $\varepsilon^p$ ). The strength properties are reduced to residual after the *critical* plastic  
416 shear strain ( $\varepsilon_{crit}^p$ ) is achieved based on the empirically derived expression [30]:

$$417 \quad \varepsilon_{crit}^p = 12.3 - (0.125 \times GSI) \quad (1)$$



418           Critical strain values in *FLAC* and *FLAC3D* are scale dependent and a  
419 model zone size adjustment can be made. For simplicity, a uniform value of  
420 critical strain was used in this model for each strain softening material across all  
421 zone sizes.

422           The trona and subsequent overlying mudstone/shale/sandstone units were  
423 modelled with the *SS* constitutive model to capture the post-peak behaviour  
424 characteristic of most of the rock units. The relatively ductile oilshale unit  
425 underlying Bed 17 was represented by a perfectly plastic *Mohr* constitutive  
426 model. In general, horizontal discontinuities (*i.e.*, bedding) were not directly  
427 represented in the numerical model; instead the *SUBI* constitutive model was used  
428 in some of the shale units. The previously described *FLAC* interfaces at the  
429 horizontal contacts between major Geotechnical Domains were assigned a  
430 perfectly plastic Mohr-Coulomb constitutive model to allow separation and/or  
431 shear between the units.

#### 432 5.1.4 Excavation Sequence

433           Excavation was simulated in two dimensions by removing the Bed 17  
434 zones representing a given panel. An interface was placed on the roof and floor  
435 within each excavated panel so that the roof and floor zones could “touch,” if  
436 required, and build-up resultant contact stresses. An internal pressure boundary  
437 was then applied to the rock mass roof/floor/walls equal to the initial pre-  
438 excavation pressure for both the horizontal and vertical directions, thereby  
439 maintaining the initial state of equilibrium within the model. This internal  
440 pressure was then reduced in ten equal stages, cycling the model to a state of  
441 equilibrium with each stage. This technique allowed the rock mass to respond  
442 gradually to excavation without the “shock” and resulting artificial numerical  
443 yielding of instantaneous removal of the panel material [5] allowing for a pseudo-  
444 static response. This approach staged pressure reduction also simulates, to some  
445 extent, the three-dimensional aspect of excavation advance whereby the rock  
446 mass at any given point “feels” the effect of the excavation face approach and

447 then pass before finally relaxing to a state of fully-excavated equilibrium. This  
448 approach was used for each panel excavation until all four were excavated from  
449 east to west. Modelling was carried out using *FLAC*'s "large strain mode" where  
450 gridpoint coordinates were updated continually with model advance [5].

## 451 **5.2 Model Calibration and Verification**

452 As mentioned previously, numerous past modelling studies have been  
453 carried out to evaluate various mining/rock mechanics conditions throughout the  
454 Green River area mines. As a result, there is a reasonable level of understanding  
455 of both mechanisms and geotechnical conditions (*i.e.*, *in situ* stress and  
456 mechanical behaviour of geomaterials). However, the data available from the NW  
457 District longwall mining presented a unique opportunity for Solvay Mine to  
458 calibrate a numerical model to a high level of refinement.

### 459 **5.2.1 Calibration Procedure**

460 Numerous analyses were carried out to calibrate the *FLAC* model and the  
461 results indicated that the brittleness of the sandstone and shale units significantly  
462 impacted the model, resulting in distinctly different characteristic model  
463 behaviour. With properties that were too ductile, it was found that insufficient  
464 yielding of the Tower Sandstone occurred resulting in a subsidence trough with an  
465 insufficient magnitude of maximum subsidence compared to the actual response.  
466 Alternatively, with properties that were too brittle, it was found that yielding was  
467 pervasive through the Tower Sandstone resulting in a subsidence trough that was  
468 excessively steep with an excessive magnitude of maximum total subsidence.  
469 Moreover, for overly brittle conditions a clear trend showing the surface  
470 expression of the chain pillars was apparent. This characteristic was not observed  
471 in the actual field measurements (see Fig. 4). Therefore, the appropriate  
472 brittleness parameters were somewhere in between these two characteristic  
473 responses, and this was the key model parameter requiring calibration.

474           The material properties for the Geotechnical Domains (*FLAC* input  
475 parameters) were based on those described in Section 3. At least two-dozen  
476 difference *FLAC* simulations were run in order to arrive at a model that seemed to  
477 best match the instrumentation data and the observations of mining response in  
478 the NW District. Some of the key conditions that were explored in the calibration  
479 study were: the thickness of the Tower Sandstone; variation in the constitutive  
480 models; the strength parameters; and the post-peak strain softening behaviour.

481           There was some uncertainty regarding the thickness of the Tower  
482 Sandstone in the NW District. Models were run with a thickness of 43 m and  
483 83 m. Models were run with both an *SS* constitutive model and with a more  
484 sophisticated *SUBI* constitutive model for the shale units to represent the  
485 pervasive bedding within those units. There was some uncertainty in the strength  
486 parameters of the rock units. The initial model parameters were based on previous  
487 modelling studies, but were refined based on the overall model response. In  
488 particular, the cohesive strength of the shales and sandstone units were varied  
489 within the range of expected values for each unit (see Table 2). The post-peak  
490 strength parameter  $\varepsilon_{crit}^p$  was varied, particularly the value for the Tower  
491 Sandstone, in order to “fine tune” the Calibrated Model. Equation (1) was used as  
492 a starting point for  $\varepsilon_{crit}^p$  (as a function of *GSI*) and further calibration was done by  
493 applying a *factor* to those initial  $\varepsilon_{crit}^p$  values without zone size correction.

494           Fig. 8 shows model-predicted subsidence profiles (shown after excavation  
495 of all four panels only) compared to actual measurements for a select number of  
496 representative *FLAC* model calibration case runs, of the more than two-dozen  
497 runs. A summary of the analysis details and results for the four Calibration Cases,  
498 corresponding to the data plotted in Fig. 8, is provided in Table 3.

499

500 **Table 3. Summary of Calibration Cases**

Calibration Case	Analysis details	Comments about results
1	Initial rock mechanics parameters (strength and brittleness) were used with a thin Tower Sandstone unit (43 m thick).	The subsidence profile showed yielding through the tower and the imprint of the pillars was clearly visible.
2	Initial rock mechanics parameters with a thick Tower Sandstone (83 m) using the SS model for shales.	The model resulted in limited yielding of the Tower and significantly under-predicted the subsidence magnitude.
3	Thick Tower with reduced strength of the shale and increased strength of the Tower. Using the SS model for shale above Tower and <i>SUBI</i> model for the shale below the Tower.	The model resulted in limited yielding of the Tower and under-predicted the subsidence magnitude.
4	Thick Tower unit using the <i>SUBI</i> model for all shale units, refined strength parameters and increased brittleness ( <i>i.e.</i> , reduced $\varepsilon_{crit}^p$ ).	The model results show a very good match of the measured subsidence, in particular the <i>progression</i> of subsidence with mining of each panel.

501 Calibration Case 4 was deemed to be the best match, on the basis of  
 502 subsidence alone, and was considered to be the “Calibrated Model.” Moreover,  
 503 the thicker Tower Sandstone unit and use of the *SUBI* model for the shale units  
 504 has a geological justification. A more detailed comparison of the Calibrated  
 505 Model with the field data is provided in the following sections. The constitutive  
 506 models and material parameters determined for each of the Geotechnical Domains  
 507 for the Calibrated Model are summarized in Table 4.  
 508

509 **Table 4. Input parameters for *FLAC* Calibrated Model**

Geotechnical Domain	Constitutive Model	Bulk's Modulus (MPa)	Shear Modulus (MPa)	Peak		Residual	
				Cohesion (kPa)	Friction Angle (°)	Cohesion (kPa)	Friction Angle (°)
Lower Shale	<i>MOHR</i>	980	535	575	28	0	25
Oilshale Floor	<i>MOHR</i>	145	65	250	20	0	25
Bed 17 Trona	<i>SS</i>	3055	1655	1340	49	0	25
Roof Shale	<i>SUBI</i>	980	535	290	28	0	25
D Sandstone	<i>SS</i>	1225	925	1150	37	0	30
Upper Wilkins	<i>SUBI</i>	980	535	290	28	0	25
Peak							
Tower Sandstone	<i>SS</i>	1225	925	1150	37	0	30
Laney Shale/Bridger Formation	<i>SUBI</i>	980	535	290	28	0	25

510 The discontinuity properties in the Calibrated Model, representing bedding  
511 planes that were accounted for using *FLAC* interfaces and the joint properties of  
512 the *SUBI* model, were: peak cohesion = 0.5 MPa and peak friction = 18°; with  
513 residual cohesion = 0 and residual friction = 18°.

#### 514 5.2.2 Subsidence Comparison

515 Surface subsidence measurements are particularly useful for model  
516 calibration because they can be directly measured with conventional geodetic  
517 methods from ground surface with a high level of confidence. Because the unique  
518 stratigraphic profile (*i.e.*, Tower and D Sandstone units, and a trona seam with an  
519 oilshale floor) significantly affects the overall rock mass response to mining,  
520 subsidence measurements *include* the effects of the individual units (*system*  
521 *response*). Given a reasonable confidence level in the characteristics of the

522 individual units, it is this system response that is most important to calibrate in the  
523 model.

524         The results of the fully mined calibrated *FLAC* model showing vertical  
525 displacement and model yielding is shown in Fig. 9 and the resulting model-  
526 predicted subsidence profile is shown in Fig. 10. As a result of longwall panel  
527 mining, yielding occurs in the pillar/abutment sidewalls and weak oilshale floor.  
528 As the roof relaxes downward, tensile yielding occurs at the roof-pillar  
529 intersection corner and the pillar center. Shear yielding begins to develop at the  
530 panel edge moving upwards through the roof shale. The shear yielding seems to  
531 temporarily “jump” the D Sandstone and re-occur in the Upper Wilkins Peak.  
532 Eventually, the D Sandstone and overlying units yields up to the base of the  
533 Tower Sandstone and drop into the panel, leaving a gap/separation between the  
534 Upper Wilkins Peak and the Tower Sandstone.

535         The Tower Sandstone bends and begins to yield in tension above the  
536 panel. The development of a gap (separation) at the base of the Tower in  
537 combination with model-predicted tensile yielding within the bottom of the  
538 Tower, indicates that dilation of the rock mass occurred. The continued bending  
539 of the Tower induces tensile yielding in the upper portion of the Tower, above the  
540 pillar sections. This combination of tensile yielding on opposite sides of the  
541 Tower “beam” reduces the effective thickness of the beam, thereby increasing its  
542 tendency for bending. Once the Tower has yielded through, a chimney-type  
543 mechanism occurs in the upper units with greatly increased surface subsidence.  
544 This can be seen above Panel 1W2N in Fig. 9. Board and Damjanac [11] also  
545 described observing a similar mechanism for longwall mining at Solvay. A fully  
546 connected vertical line of yielded elements forms at the western edge of panel  
547 1W4N that results in concentrated vertical displacement likely as a result of the  
548 east-to-west mining sequence used in the simulation.

549         Subsidence profiles labeled 2005A and 2005B in Fig. 10 were measured  
550 when 2.5 panels were excavated (see Fig. 3). The model subsidence profiles

551 corresponding to 2 (1W2N) and 3 (1W3N) excavated panels bracket the measured  
552 results for the 2005 profiles. Although the measured values are somewhat steeper  
553 on the east side than the calibrated model results, a good match to the data was  
554 achieved. The 2006 measured profile should correspond with the three mined  
555 panels stage (1W3N). The maximum magnitude of subsidence was within about  
556 10% of the measured value and matched the trend on the east side of the model  
557 well; however, the west side model-predicted subsidence did not show as good a  
558 match.

559         The most notable difference between the model and the measured data  
560 was that the model appears to “hang up” in a small portion above the 1W2N –  
561 1W3N chain pillar. This resulted in a kink in the left side of the subsidence  
562 trough, reducing the maximum magnitude of subsidence at this stage. Yielding  
563 did not seem to pass completely through the Tower Sandstone above Panel 1W3N  
564 as it did above Panel 1W2N (see Fig. 9), and this seems to be responsible for the  
565 observed effect. This could be due to the limitations of the two-dimensional  
566 model geometry, mining sequence simulation, or the constitutive model.  
567 However, this difference was relatively minor and the properties used in this  
568 model have provided an overall strong match to observations.

569         Development of the failure mechanism that results in this Calibrated  
570 Model response is shown in Fig. 11. After mining a single panel (Fig. 11a),  
571 inclined shearing bands develop at the panel edge resulting in minor surface  
572 subsidence (15 cm predicted). After a second panel was mined (Fig. 11b) a  
573 yielding mechanism developed due to interaction of the two mined panels that  
574 allowed for movement of the material above the inter-panel pillar into the gob  
575 with resulting increased surface subsidence (52 cm predicted). Load shedding  
576 from the inter-panel pillars to the gob material can be expected with this type of  
577 yielding mechanism.

578 5.2.3 *Pillar Stressmeter Measurement Comparison*

579 Basic calibration of the numerical model was primarily done using the  
580 subsidence measurements and past experience modelling studies at Solvay Mine,  
581 as described in the previous section. The stressmeter data provided an opportunity  
582 to compare the longwall panel-scale instrumentation data to the model. However,  
583 it should be stated that stressmeter data can be heavily influenced by localized  
584 influences, such as fracture formation, especially in high stress zones. The model  
585 with parameters that resulted in the best match of subsidence was compared with  
586 the stress measurements described in Section 4.2 to further evaluate the  
587 calibration.

588 The model indicated that unloading occurs above the excavated panels  
589 with vertical pressure of up to nearly 13.8 MPa in the gob. Maximum vertical  
590 stresses of approximately 34.5 MPa occur in the pillars and abutments. The  
591 stresses after mining all panels agrees well with a simplified tributary area  
592 estimate of  $\sigma_p = 35.1$  MPa from the following equation [31]:

593 
$$\sigma_p = \gamma z \left( 1 + \frac{w_o}{w_p} \right) \quad (2)$$

594 Where:

595  $\sigma_p$  - average vertical pillar stress

596  $\gamma$  - unit weight of rock mass (0.025 MN/m<sup>3</sup>)

597  $z$  - depth below ground surface to pillar mid-height (470 m)

598  $w_p$  - width of pillar (83 m)

599  $w_o$  - width of opening (165 m)

600 In the model, vertical stress within the east side of the chain pillars is  
601 lower than the west side due to the east-to-west excavation sequence that induced  
602 yielding on the east portion of the pillars before higher stresses concentrate on the  
603 west side. This results in asymmetrical loading on the pillars with mining  
604 advance. Addressing this stress progression is one of the strengths of numerical



605 modelling analysis. The evolution of vertical stress was recorded throughout the  
606 model runs (*i.e.*, as the model cycled through all stages of excavation) at locations  
607 within the model corresponding as closely as possible to the stressmeter locations  
608 to allow for comparison between model and actual measurements.

609 As a means of comparison between actual and model stresses, the average  
610 vertical stress change for the instruments, grouped by location, is shown in  
611 Fig. 12. There was no instrumentation data to match Stage 1 (one panel mine and  
612 prior to instrumentation installation). This plot shows that the model and field  
613 measurements are an overall good match for Stage 2 (after two panels were  
614 mined). At Stage 3 (after three panels were mined) the trends do not match,  
615 particularly at Area C where the instrumentation shows significantly greater stress  
616 levels. No instrumentation data was available for Stage 4 (after all panels were  
617 mined); however, as mentioned above the model achieved a reasonable match to  
618 tributary area theory at this final stage of mining.

619 At Area C, data for only one IRAD stressmeter location was available for  
620 comparison at Stage 3 where the greatest discrepancy occurs. The “hang up” in  
621 this region of the model discussion in Section 5.2.2 contributes to some of the  
622 discrepancy. The average measured vertical stress change at Area C was about  
623 40 MPa, which is 7% higher than the total maximum vertical stress in the pillar.  
624 Based on the *FLAC* model-predicted stresses, and observations of good gate pillar  
625 performance, it seems unlikely that stress change at this location could approach  
626 the measured value of 41 MPa. If the pre-mining *in situ* vertical stress of  
627 12.4 MPa is added to the measure stress change of 41 MPa, this would result in  
628 total vertical stresses of nearly 55.2 MPa at Area C during Stage 3. Based on the  
629  $UCS = 45$  MPa for Bed 17 trona, and the measured vertical stresses at Area C, the  
630 ratio of vertical pillar stress ( $\sigma_p$ ) to  $UCS$  is greater than 1. Based on established  
631 pillar strength relations such as Lunder and Pakalnis [32], for a width-to-height  
632 ratio of about 14, significant stress-induced instability (*i.e.*, shearing / crushing /  
633 spalling) could be expected in the pillars. The pillar damage predicted by the Area

634 C recorded stresses was *not* observed within pillars at this location in the mine;  
635 therefore, it seems reasonable to conclude that the measured stress change at Area  
636 C after 2 panels were mined is likely incorrect or strongly affected by localized  
637 conditions, and that stresses from the model are within expected values. Likewise,  
638 the stressmeters at Area A (lower than anticipated magnitudes) are likely also  
639 impacted by localized fracturing and pillar yielding.

## 640 **6. Three-Dimensional Back Analysis of SW District Longwall**

641 Based on a comparison of subsidence, stress measurements and mining  
642 observations, a reasonable calibration of the *FLAC* model appears to have been  
643 achieved. The main purpose of the calibration exercise was to develop a *FLAC*  
644 model suitable to verify and refine the design of additional longwall panels in the  
645 SW District (see Fig. 1). A two-dimensional *FLAC* model of the SE District  
646 longwall panels was developed for a first stage design evaluation; however, the  
647 results of the two-dimensional analysis will not be discussed in this paper.

648 The two-dimensional analyses discussed thus far have been useful because  
649 various analyses could be carried out rapidly for the calibration study and the  
650 interpretation was reasonably straightforward. However, longwall mining  
651 advance is truly a three-dimensional problem; therefore, three-dimensional  
652 analyses using *FLAC3D* were conducted to compliment the two-dimensional  
653 models and provide further insight into mining performance. The main purpose  
654 of the three-dimensional analysis was to evaluate panel design dimensions for the  
655 SE District where the Tower Sandstone is thinner and where the depth from  
656 ground surface to Bed 17 is greater, compared to the NW District. In particular, to  
657 determine if reduced chain pillar width and increased longwall panel width would  
658 result in mining performance significantly different from that of the NW District  
659 longwalls.

660 At the time of the analysis the westernmost panel of the SE District had  
661 been mined (see Fig. 1). Because of the presence of TDR cable in a borehole

662 located in the first mined panel (see Fig. 5) of the SE District, this provided an  
663 opportunity to further validate the Calibrated Model assumptions in a three-  
664 dimensional model.

665 The three-dimensional model geometry was similar to the two-  
666 dimensional model with similar zone sizes and aspect ratios. The aspect zone  
667 ratios were typically 1:1:1 (z-vertical:x-horizontal:y-horizontal) in the critical  
668 strain softening units, such as the Tower Sandstone; 1:2:2 in some of the shale  
669 units; and up to 1:4:4 in the Oilshale where perfectly plastic post-peak behaviour  
670 makes zone aspect ratio of lesser importance. The material properties and  
671 constitutive models that were calibrated in *FLAC* were also used in the *FLAC3D*  
672 model. Again, interfaces were included between major geological units to allow  
673 for separation and potential bulking behaviour. In order to increase calculation  
674 efficiency, the upper strata *above* the Tower Sandstone was not directly modelled,  
675 but instead was represented by a uniform pressure equal to the weight of the  
676 equivalent overburden. Use of symmetry boundary conditions was made along  
677 vertical planes through the middle of the panels oriented east-west (normal to  
678 panel direction) and north-south. The mining of three panels could be efficiently  
679 simulated this way. The model geometry showing stratigraphy is shown in  
680 Fig. 13.

681 Excavation of each panel in a manner similar to that carried out in the two-  
682 dimensional analyses was considered to be a practical simplification (*i.e.*,  
683 instantaneous excavation of each panel). This was done by removing the panel  
684 material and replacing it with stabilizing reaction forces that were reduced in ten  
685 equal stages until the excavation-induced stresses had been completely “relaxed”  
686 to a state of final equilibrium. The westernmost panel that was mined prior to the  
687 modelling exercise had a panel width of 190 m. In order to evaluate mine  
688 dimensions, *FLAC3D* models with panel widths of 190, 198 and 213 m, all with  
689 gross pillar widths of 82 m (39-m-wide chain pillars), were analyzed. In addition,

690 a reduced pillar width model with gross pillar width of 73 m (34-m-wide chain  
691 pillars) was analyzed for a 190 m panel width.

692 A plot showing a section through the centre of the westernmost SE District  
693 longwall panel is shown in Fig. 14. This plot shows that the panel stayed open  
694 until 30 m of model face advance (or 60 m of actual excavated panel length due to  
695 the symmetry assumptions), before roof collapse due to delamination of the roof  
696 shale from the D Sandstone. After 107 m of advance (214 m of open symmetrical  
697 excavation), a gap can be seen in the model between the D Sandstone and the roof  
698 shale, indicating delamination near the face. At the same advancement distance  
699 the D Sandstone and Upper Wilkins Peak formation have separated from the  
700 Tower Sandstone and fallen into the panel approximately 30 – 45 m behind the  
701 face in the model. This corresponds to a 14 – 20° angle of break from the panel  
702 face to separation at the base of the Tower Sandstone. This is in agreement with  
703 the 18 – 20° degree angle of break observed in the field based on TDR  
704 measurements of early-stage mining in the SE District (see Fig. 15). After 213 m  
705 of advance (426 m of open symmetrical excavation) in the model, yielding of the  
706 Tower Sandstone into the panel can be seen approximately 122 m behind the  
707 excavation face. This trend of initial separation below D Sandstone at the mining  
708 face, followed by delamination from the base of the Tower Sandstone and then  
709 collapse of the Tower Sandstone, continues for the remainder of the panel  
710 excavation. No large “hang-up” of the Tower Sandstone followed by a significant  
711 collapse (i.e., delayed failure) seems to occur with the dimensions and  
712 stratigraphy used in the simulation.

713 The agreement with TDR measurements, using a three-dimensional model  
714 based on assumptions from the two-dimensional calibrated model, is particularly  
715 compelling support for the validity of the calibration assumptions.

716 **7. Summary and Conclusions**

717 An integrated design program utilizing instrumentation and monitoring,  
718 along with numerical modelling has been used by Solvay Mine and their rock  
719 mechanics consultant Itasca Consulting Group, Inc. for more than two decades.  
720 Over that time, qualitative and quantitative (*i.e.*, instrumentation monitoring)  
721 observations of the ground response to mining, at the scale of mine  
722 openings/pillars up to overall regional mine-scale have been collected. These  
723 observations have been used to continually refine predictive numerical models.  
724 The models suitably captured the complex behaviour of the mine due to the  
725 significant contrasts in the mechanical properties of the stratigraphic units,  
726 particularly the massive Tower Sandstone.

727 Longwall mining carried out in the NW and SE Districts of Solvay Mine  
728 presented an excellent opportunity to develop and validate calibrated two- and  
729 three-dimensional models. Model input parameters (*e.g.*, strength of various units)  
730 were available from numerous past modelling studies and the calibration exercise  
731 carried out in this study indicated that the most critical parameters required for  
732 calibration were the post-peak strain softening parameter  $\varepsilon_{crit}^p$  (*i.e.*, brittleness) of  
733 the units. After conducting more than two dozen *FLAC* models as part of this  
734 study, a Calibrated Model was arrived at that provided a strong match to  
735 instrumentation data, particularly surface subsidence, and mining observations.  
736 Moreover, a three-dimensional *FLAC3D* model using the calibration assumptions  
737 was able to capture TDR observations of behaviour within the stratigraphic units.

738 The calibrated two- and three-dimensional models were able to provide a  
739 reasonable match to actual ground surface subsidence, in-seam (Bed 17) pillar  
740 stresses, and TDR measurements. By obtaining a reasonable match of the  
741 measured field data throughout the stratigraphy and in both two and three  
742 dimensions, a well-calibrated model was developed. The consistent similarity in  
743 rock mechanics mechanisms and instrumentation data between field observations  
744 and the Calibrated Model allow Solvay Mine to utilize numerical-modelling as

745 part of an ongoing mine design involving more complex conditions (*e.g.*, solution  
746 and room-and-pillar mining).

747           On the basis of the understanding of conditions and mechanisms gained  
748 from this study, future work can include additional complexities. For example,  
749 larger scale and more detailed three-dimensional modelling, direct modelling of  
750 gob development and greater refinement of geotechnical conditions (*e.g.*, *in situ*  
751 stresses and material properties).

## 752 **Acknowledgements**

753           The authors would like to thank Solvay Minerals for permission to publish  
754 this work and, in particular, Ron Hughes, who was Solvay Mine Manager at the  
755 time that this work was conducted. Both of the authors were employees of Itasca  
756 Consulting Group, Inc. at the time this work was done and would like to thank  
757 them for their support. Numerous other engineers shared their insights and  
758 experience with numerical modelling of trona mining, most notably, Branko  
759 Damjanac and Matt Pierce of Itasca Consulting Group, Inc. Judy MacLean and  
760 Kathy Sikora both kindly assisted with editing the manuscript, and Jonatan  
761 Perrier-Daigle assisted with figure preparation.

762    **References**

763    [1] Pechmann JC, Walter WR, Nava SJ, Arabasz WJ. The February 3, 1995, ML  
764    5.1 seismic event in the Trona Mining District of southwestern Wyoming.  
765    Seismol Res Lett 1995; 66:25-34.

766    [2] Zipf RK, Swanson P. Description of a large catastrophic failure in a  
767    southwestern Wyoming trona mine. In: Amadei, Kranz, Scott, Smealie, editors.  
768    Rock Mechanics for Industry: Balkema, Rotterdam; 1999, p. 293-298.

769    [3] Board M, Damjanac B, Pierce M. Development of a methodology for analysis  
770    of instability in room and pillar mines. Deep Mine 07, Proceedings of the Fourth  
771    International Seminar on Deep and High Stress Mining 2007:273-82.

772    [4] Whyatt J, Varley F. Catastrophic failures of underground evaporite mines.  
773    Proceedings: 27th International Conference on Ground Control in Mining  
774    2008:29-31.

775    [5] Itasca Consulting Group Inc. *FLAC* (Fast Lagrangian Analysis of a Continua)  
776    User's Manual, Version 5.0. 2005.

777    [6] Itasca Consulting Group Inc. *FLAC3D* (Fast Lagrangian Analysis of a  
778    Continua in 3 Dimensions) User's Manual, Version 3.00. 2005.

779    [7] Corkum AG, Board MP. Analysis of Longwall Mining Layout for the  
780    Southeast District of Solvay Mine, Itasca Consulting Group Inc. Report to Solvay  
781    Mine. 2007.

782    [8] Board MP. Numerical Examination of Mechanisms of Collapse of the 1SW  
783    Panel at Solvay Mine, Itasca Consulting Group Inc. Report to Solvay Mine. 1995.

- 784 [9] Board MP. Solvay High Extraction Panel Modelling, Itasca Consulting Group  
785 Inc. Report to Solvay Mine. 1997.
- 786 [10] Board MP. Examination of the Failure Potential of the Tower Sandstone Unit  
787 in Bending, Itasca Consulting Group Inc. Report to Solvay Mine. 1998.
- 788 [11] Board MP, Damjanac B. Numerical Analysis of Caving Behaviour of the  
789 Overburden at the Proposed Longwall Panels: Solvay Mine, Green River,  
790 Wyoming, Itasca Consulting Group Inc. Report to Solvay Mine. 2001.
- 791 [12] Wiig SV, Grundy WD, Dyni JR. Trona resources in the Green River Basin,  
792 southwest Wyoming. Open-File Report - U.S. Geological Survey 1995:88.
- 793 [13] Powell JW. Report on the geology of the eastern portion of the Uinta  
794 Mountains. U.S. Geological and Geographic Survey, 2nd Division 1876:218.
- 795 [14] Ebens RJ. Tower Sandstone lenses at Green River, Wyoming. Rocky  
796 Mountain Geology 1965; 4:75-9.
- 797 [15] Culbertson WC. Stratigraphy of the Wilkins Peak Member of the Green  
798 River Formation, U.S. Geological Survey. 1961:170-3.
- 799 [16] Maleki H. Rock Mechanics Study of 624-ft Wide Face (PowerPoint Slides),  
800 Presentation to Solvay Minerals, Inc. 2006.
- 801 [17] Tetra Tek Inc. Physical and Mechanical Properties Characterization of OGT  
802 OOEX 2, Report prepared for Joint Oil/Gas & Trona Industry Development  
803 Group. 1996.
- 804 [18] Weller M. Solvay Mine: Compilation of Rock Mechanics Properties of  
805 Overburden Units, Report to Solvay Mine. 2000.



- 806 [19] Hoek E, Carranza-Torres C, Corkum B. Hoek-Brown failure criterion - 2002  
807 edition. Proceedings of NARMS-TAC 2002; 1:267-73.
- 808 [20] Esterhuizen E, Mark C, Murphy MM. Numerical model calibration for  
809 simulating coal pillars, gob and overburden response. Proceedings: International  
810 Conference on Ground Control in Mining ICGCM 2010:46-57.
- 811 [21] Hoek E, Brown ET. Empirical strength criterion for rock masses. J Geotech  
812 Eng Div 1980; 106:1013-35.
- 813 [22] Hoek E, Grabinsky MW, Diederichs MS. Numerical modelling for  
814 underground excavation design. T I Min Metall 1991; 100:A22-30.
- 815 [23] Pappas D, Mark C. Load Deformation-Behavior of Simulated Longwall Gob  
816 Material. Proceedings: 12th International Conference on Ground Control in  
817 Mining 1993:184-93.
- 818 [24] O'Connor KM, Dowding CH. Distinct element modeling and analysis of  
819 mining-induced subsidence. Rock Mech Rock Engng 1992; 25:1-24.
- 820 [25] Deb D, Park DW. Numerical modeling of progressive gob formation in a  
821 deep longwall mine. Proceedings: 2nd North American Rock Mechanics  
822 Symposium 1996; 2:1893-901.
- 823 [26] Alejano LR, Ramírez-Oyanguren P, Taboada J. FDM predictive  
824 methodology for subsidence due to flat and inclined coal seam mining. Int J Rock  
825 Mech Min Sci 1999; 36:475-91.
- 826 [27] Pierce M, Cundall P, Potyondy D, Mas Ivars D. A synthetic rock mass model  
827 for jointed rock. Proceedings: Canadian-U S Rock Mechanics Symposium 2007;  
828 1:341-9.

- 829 [28] Peng SS. Longwall mining. 2nd ed. Morgantown, WV: Department of  
830 Mining Engineering, West Virginia University, 2006.
- 831 [29] Starfield AM, Cundall PA. Towards a methodology for rock mechanics  
832 modelling. *Int J Rock Mech Min Sci* 1988; 25:99-106.
- 833 [30] Lorig LJ, Pierce ME. Methodology and Guidelines for Numerical Modelling  
834 of Undercut and Extraction-Level Behaviour in Caving Mines - International  
835 Caving Study End of Project Report (Confidential). 2000.
- 836 [31] Hoek E, Brown ET. *Underground Excavations in Rock*. London: The  
837 Institution of Mining and Metallurgy, 1980.
- 838 [32] Lunder P, Pakalnis R. Determination of the strength of hard-rock mine  
839 pillars. *Bull Can Inst Miner Metall* 1997:51-5.
- 840

841

## LIST OF TABLES

842 Table 1 Intact rock properties from Weller [19]

843 Table 2 Estimated *in situ* rock mass properties for sandstones and shales (from  
844 [17])

845 Table 3. Summary of Calibration Cases

846 Table 4. Input parameters for *FLAC* Calibrated Model

847

## LIST OF FIGURES

- 848
- 849 Fig. 1 Solvay Mine layout as of May 2007 showing NW District longwall panels  
850 used for model calibration and SE District longwall panels: the subject of the  
851 design study. The majority of mine is comprised of room and pillar panels.
- 852 Fig. 2 Stratigraphy of the NW and SE Districts are similar; however, the Tower  
853 Sandstone is substantially thicker in the SE District and the depth from  
854 surface to Bed 17 is greater in the SE District.
- 855 Fig. 3 Contours of surface subsidence (from geodetic surveying) for the NW  
856 District with mined out longwall panels superimposed (Modified from [16]).  
857 Mined out portions of the longwall panels are indicated by hatching. Sections  
858 A, B and C are identified.
- 859 Fig. 4 Measured subsidence along section lines. The section line locations are  
860 shown in Fig. 3.
- 861 Fig. 5 Location of IRAD stressmeter cells and area grouping in the NW District  
862 longwall panels.
- 863 Fig. 6 Stress measurements from IRAD stressmeters (locations shown in Fig. 5)  
864 within chain pillars in NW District (original data from [16]).
- 865 Fig. 7 *FLAC* model grid used for NW District longwall back analysis. Note that  
866 the model truncated laterally and vertically in this image.
- 867 Fig. 8 Comparison of various *FLAC* model runs, including the Calibrated Model,  
868 with actual conditions for the fully mined stage along Section C (Fig. 3).
- 869 Fig. 9 *FLAC* model results after excavation of all four longwall panels (panels  
870 excavated right to left). Yielding through the Tower Sandstone unit and  
871 active failure along the “leading edge” (left side of the model) resulted in a  
872 steep subsidence trough with up to 75 cm of subsidence. Note: negative  
873 values represent downward displacement.
- 874 Fig. 10 Comparison between field-measured and *FLAC* Calibrated Model  
875 predicted subsidence along Section C (Fig. 3).

876 Fig. 11 *FLAC* model results showing yielding and contours of cohesion (red  
877 indicates strain softening to residual cohesion). The yielding mechanism that  
878 develops due to interaction between panels results in a wedge-like shearing  
879 above inter-panel pillars associated with load shedding into the gob. Note  
880 that circles represent tensile failure and crosses represent shear failure.

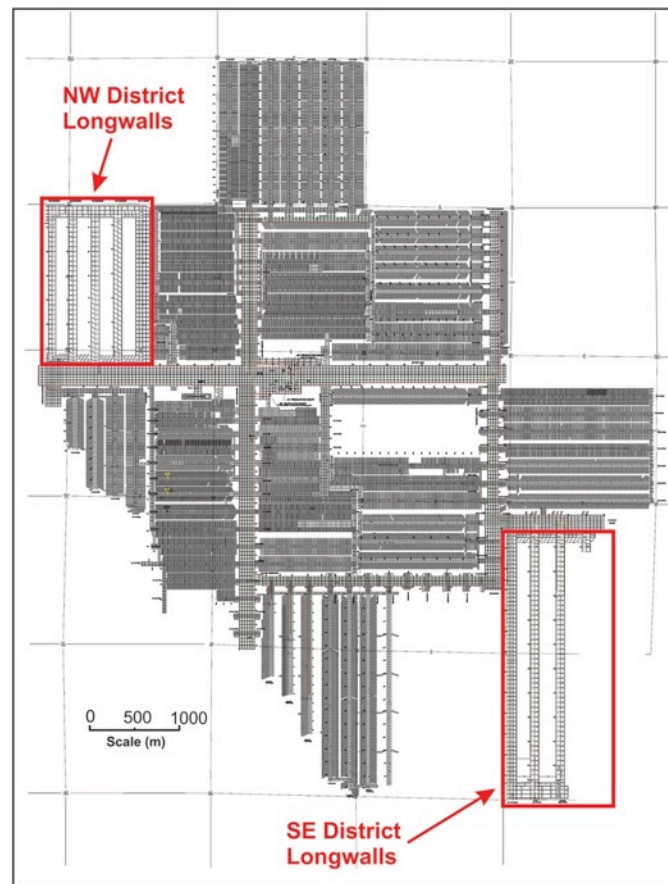
881 Fig. 12 Comparison of the average vertical stress for each area grouping (see Fig.  
882 5) from stressmeter measurements compared to *FLAC* model predicted  
883 stress.

884 Fig. 13 Geometry of the *FLAC3D* model for evaluation of longwall mining in the  
885 SE district.

886 Fig. 14 *FLAC3D* model of SE Longwall with sequential excavation advancement  
887 in 15 m-long increments. Note that because of the symmetric boundary  
888 condition (“rollers”) on the left side of the model, the excavation length is  
889 twice that shown in the model. The “true” excavation length is shown in the  
890 figure labels.

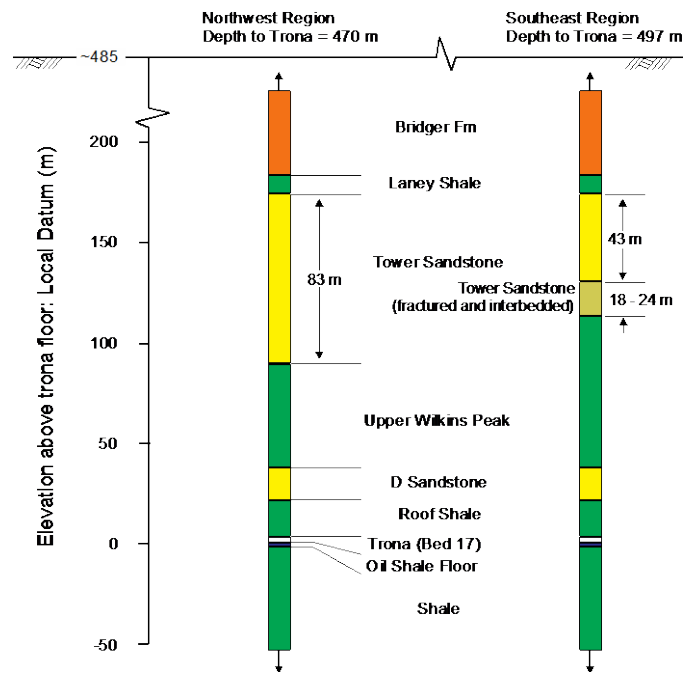
891 Fig. 15 Observations of bed separation from TDR instrumentation located in the  
892 westernmost longwall panel in the SE District (see Fig. 5).

893



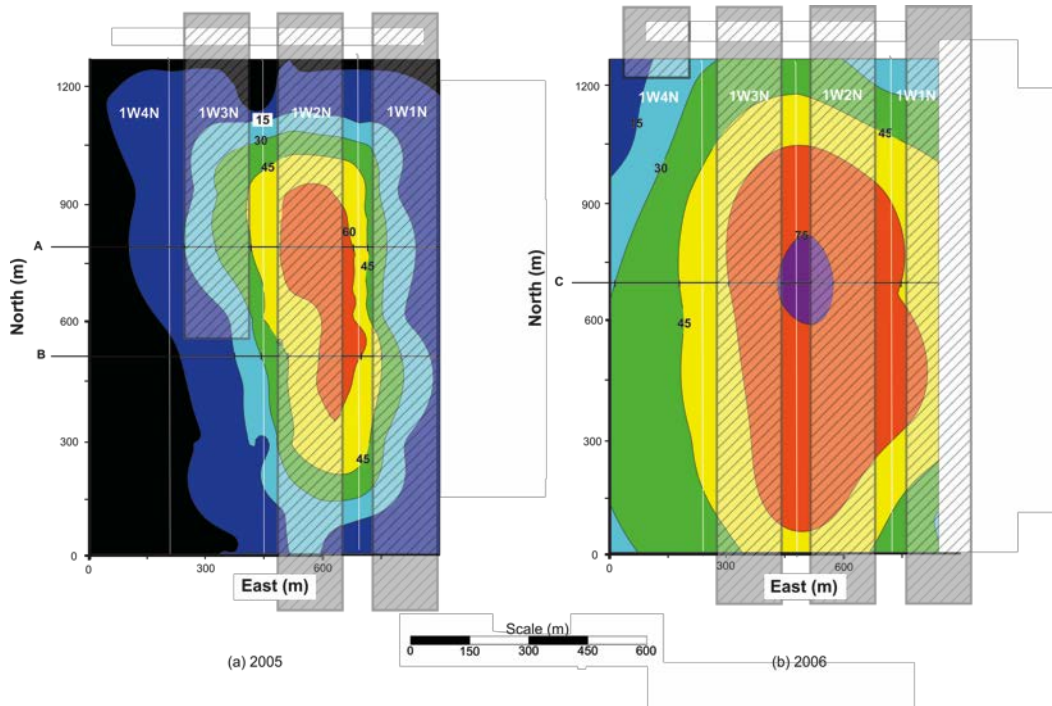
895

896 **Fig. 1 Solvay Mine layout as of May 2007 showing NW District longwall panels used**  
897 **for model calibration and SE District longwall panels: the subject of the design**  
898 **study. The majority of mine is comprised of room and pillar panels.**



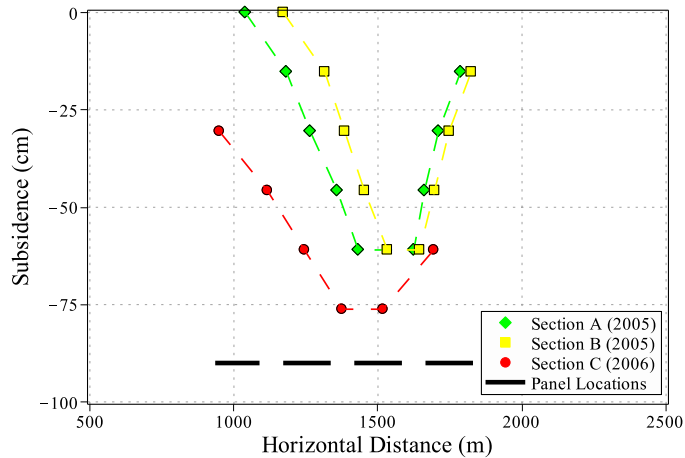
899

900 **Fig. 2 Stratigraphy of the NW and SE Districts are similar; however, the Tower**  
 901 **Sandstone is substantially thicker in the SE District and the depth from surface to**  
 902 **Bed 17 is greater in the SE District.**



903

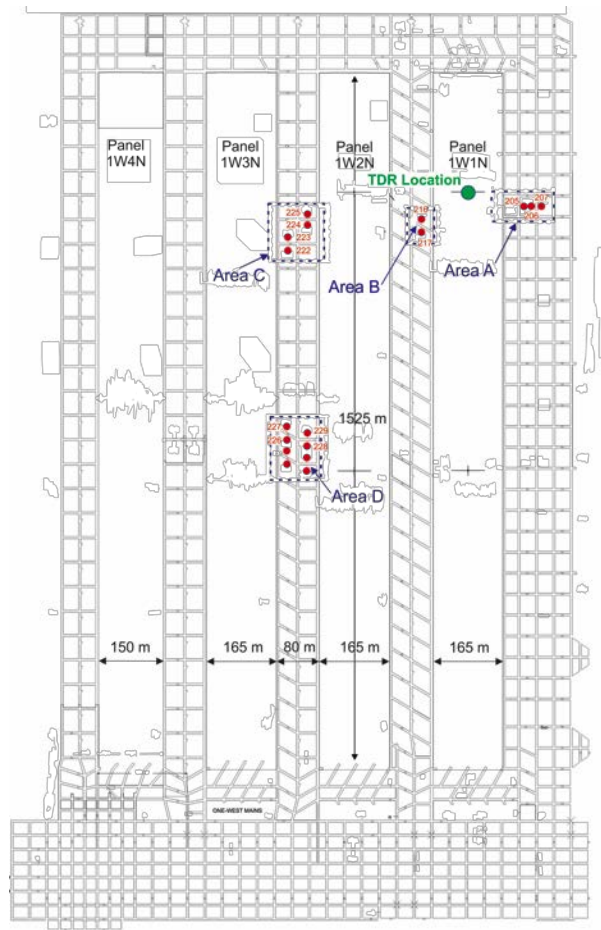
904 **Fig. 3** Contours of surface subsidence (from geodetic surveying) for the NW District  
 905 with mined out longwall panels superimposed (Modified from [16]). Mined out  
 906 portions of the longwall panels are indicated by hatching. Sections A, B and C are  
 907 identified.



908

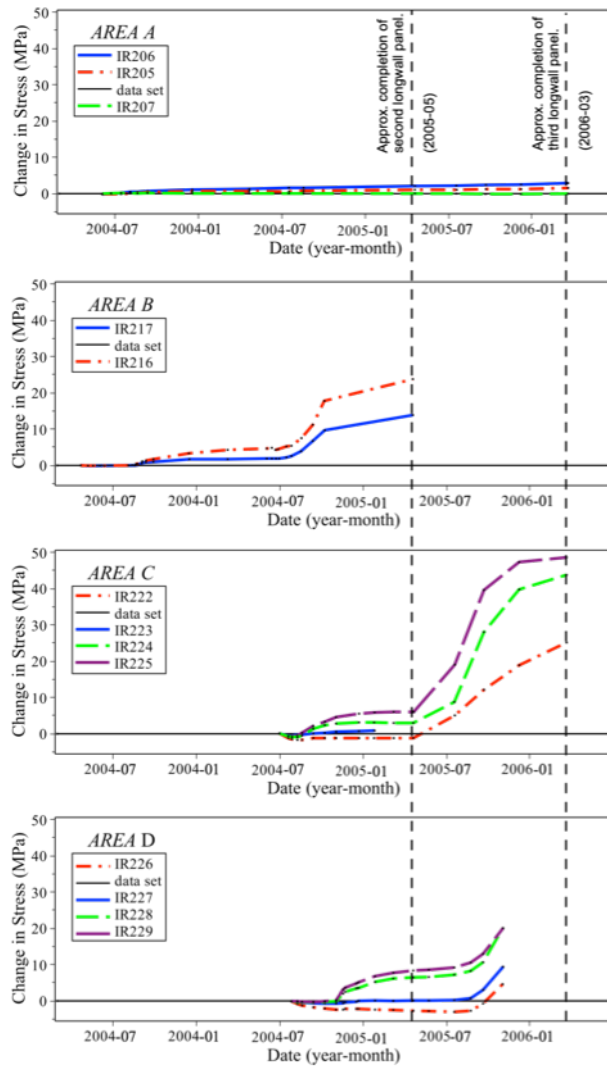
909 **Fig. 4** Measured subsidence along section lines. The section line locations are shown  
 910 in Fig. 3.





911

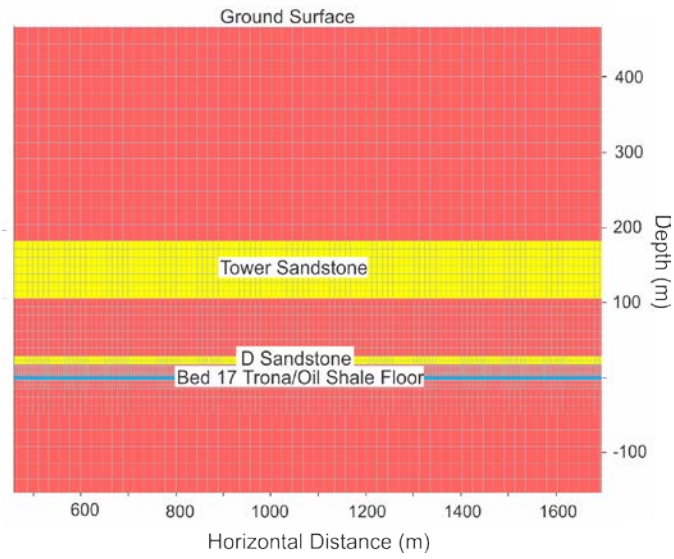
912 **Fig. 5 Location of IRAD stressmeter cells and area grouping in the NW District**  
 913 **longwall panels.**



914

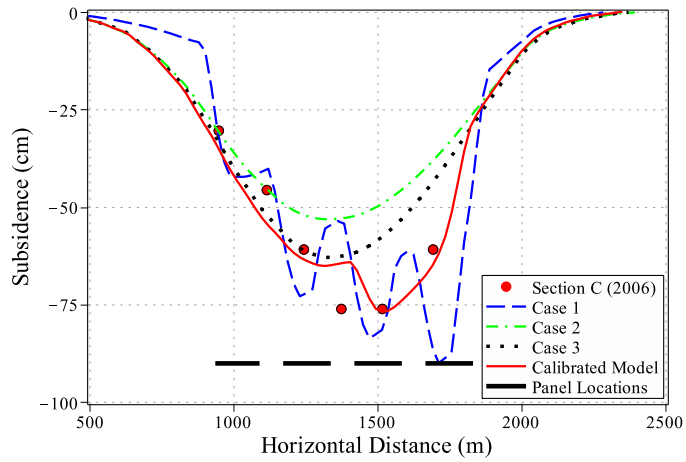
915 **Fig. 6 Stress measurements from IRAD stressmeters (locations shown in Fig. 5)**

916 **within chain pillars in NW District (original data from [16]).**



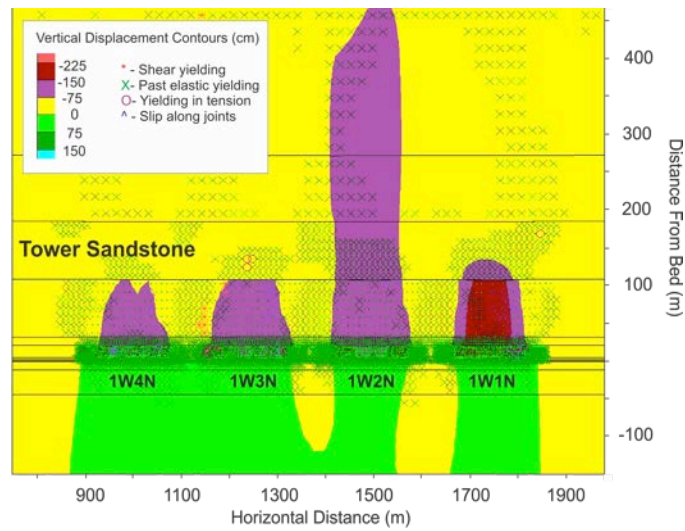
917

918 **Fig. 7** *FLAC* model grid used for NW District longwall back analysis. Note that the  
 919 model truncated laterally and vertically in this image.



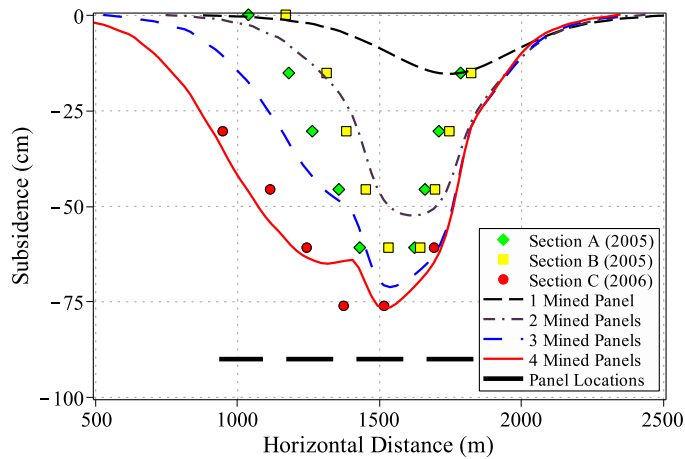
920

921 **Fig. 8** Comparison of various *FLAC* model runs, including the Calibrated Model,  
 922 with actual conditions for the fully mined stage along Section C (Fig. 3).



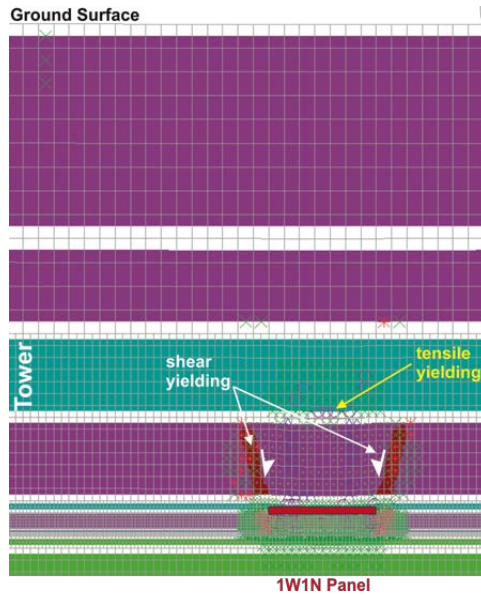
923

924 **Fig. 9** *FLAC* model results after excavation of all four longwall panels (panels  
 925 excavated right to left). Yielding through the Tower Sandstone unit and active  
 926 failure along the “leading edge” (left side of the model) resulted in a steep  
 927 subsidence trough with up to 75 cm of subsidence. Note: negative values represent  
 928 downward displacement.

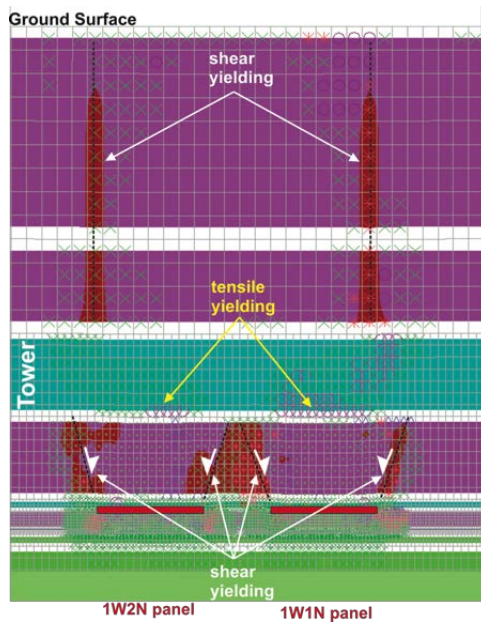


929

930 **Fig. 10** Comparison between field-measured and *FLAC* Calibrated Model predicted  
 931 subsidence along Section C (Fig. 3).

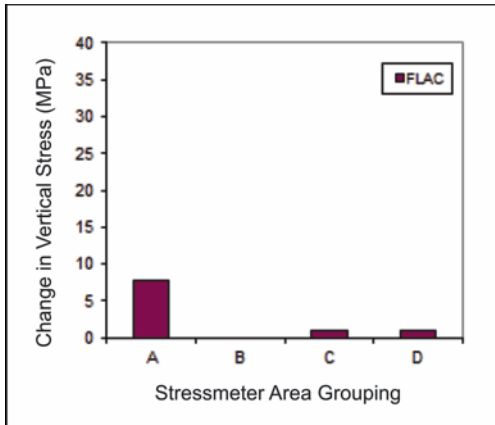


(a) Single panel mined with a maximum predicted subsidence of 15 cm.

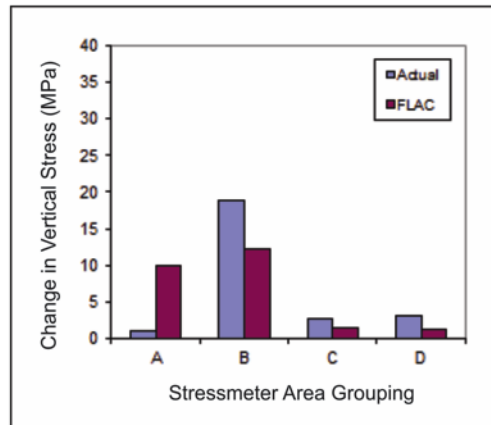


(b) Two panels mine with maximum subsidence of 52 cm.

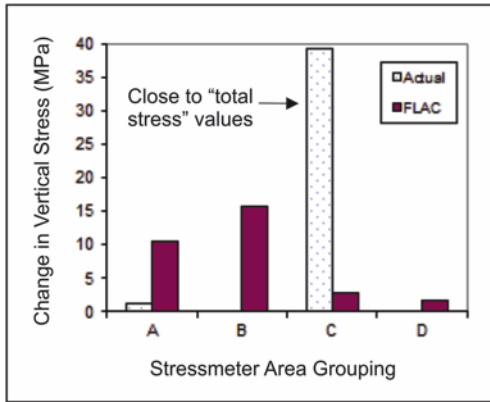
932 **Fig. 11** *FLAC* model results showing yielding and contours of cohesion (red indicates  
 933 strain softening to residual cohesion). The yielding mechanism that develops due to  
 934 interaction between panels results in a wedge-like shearing above inter-panel pillars  
 935 associated with load shedding into the gob. Note that circles represent tensile failure  
 936 and crosses represent shear failure.



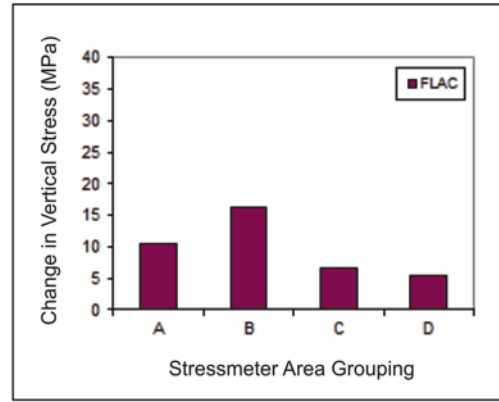
(a) Stage 1:1 panel excavated



(b) Stage 2:2 panels excavated



(c) Stage 3:3 panels excavated

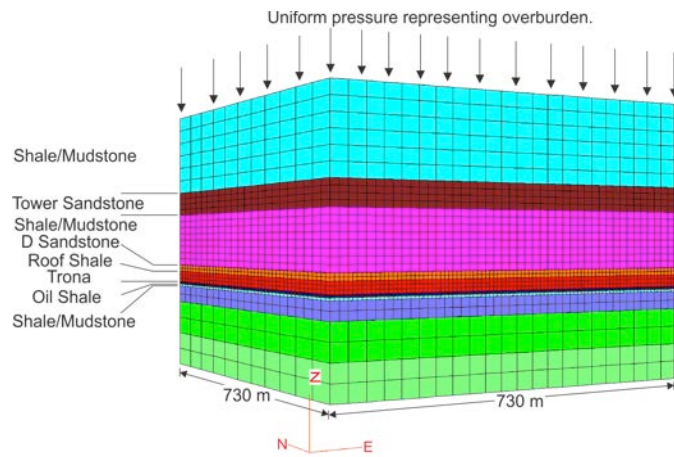


(d) Stage 4:4 panels excavated

937

938 **Fig. 12 Comparison of the average vertical stress for each area grouping (see Fig. 5)**

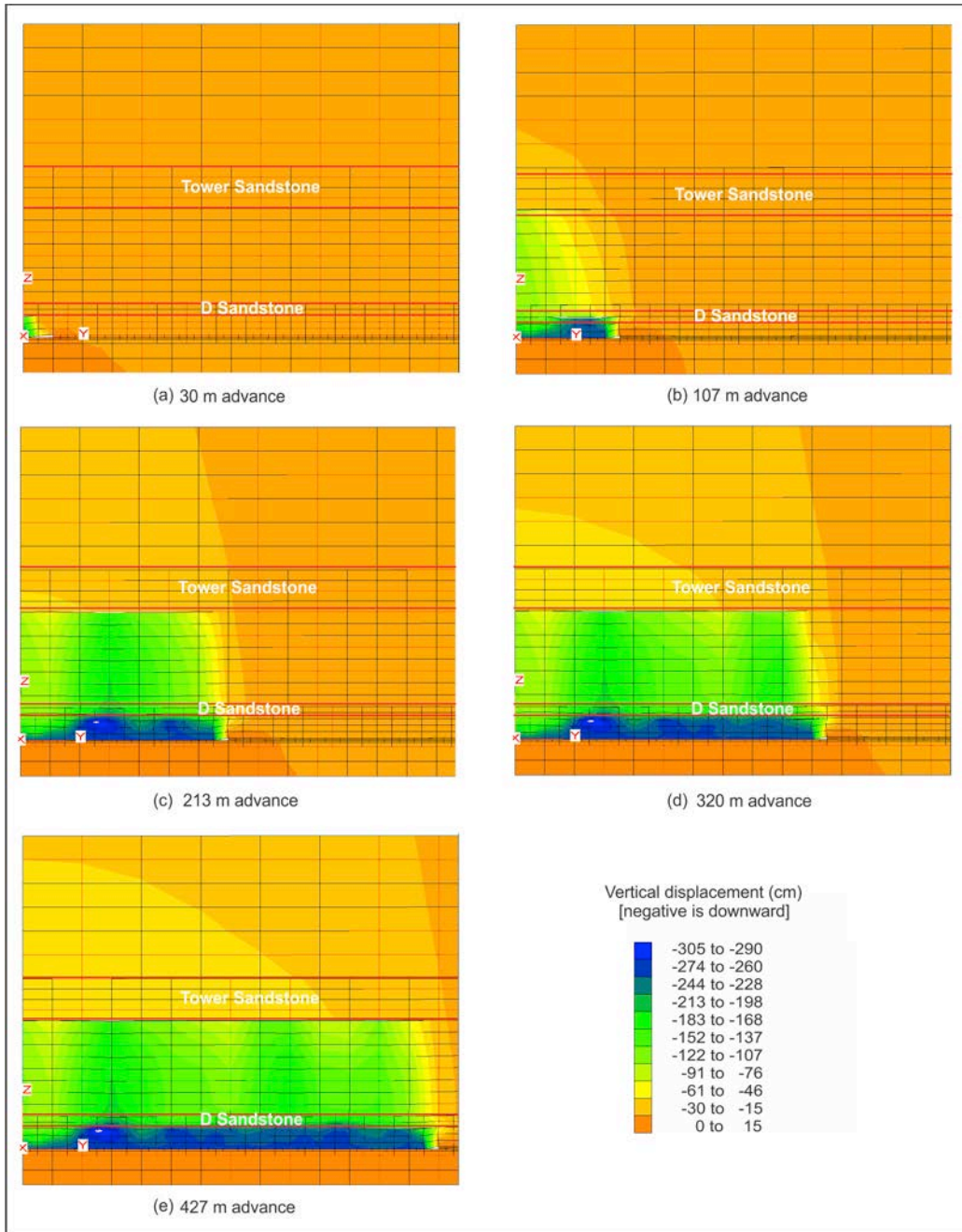
939 **from stressmeter measurements compared to *FLAC* model predicted stress.**



940

941 **Fig. 13 Geometry of the *FLAC3D* model for evaluation of longwall mining in the SE**

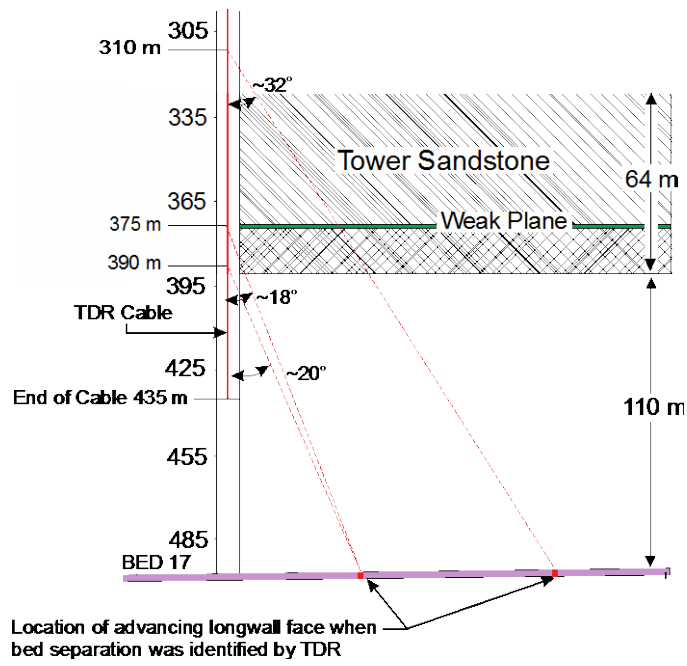
942 **district.**



943

944 **Fig. 14** *FLAC3D* model of SE Longwall with sequential excavation advancement in  
 945 **15 m-long increments. Note that because of the symmetric boundary condition**  
 946 **(“rollers”) on the left side of the model, the excavation length is twice that shown in**  
 947 **the model. The “true” excavation length is shown in the figure labels.**





948

949 **Fig. 15 Observations of bed separation from TDR instrumentation located in the**  
 950 **westernmost longwall panel in the SE District (see Fig. 5).**

951